Available online at www.sciencedirect.com
SCIENCE DIRECT®
Journal of Sound and Vibration 280 (2005) 983–995
JOURNAL OF SOUND AND VIBRATION
www.elsevier.com/locate/jsvi

Stepwise approximation of an optimally flared tunnel portal

A. Winslow, M.S. Howe*

College of Engineering, Boston University, 110 Cummington Street, Boston, MA 02215, USA

Received 5 September 2003; accepted 5 January 2004
Available online 15 September 2004

Abstract

An optimally flared tunnel portal causes the pressure to rise linearly across the front of the compression wave generated by an entering high-speed train. The wave front thickness $\sim \ell/M$ when the flared section has length ℓ and the train Mach number is M. The flared portal would likely be constructed in practice using a set of coaxial cylindrical sections that together approximate the ideal flared geometry. A numerical study is described in this paper to determine how these discrete sections modify the generation of the compression wave. The interaction of train nose 'sources' with successive changes in portal diameter produces a 'rippling' of the pressure wave profile. Our results show how the amplitude of these fluctuations depends on the length of the train nose and on the number of cylindrical sections, and suggest that an ideally flared portal is well approximated by a stepped-portal fabricated from three or four sections. The results are applicable for train Mach numbers up to about 0.25 ($\sim$ 300 kph).

1. Introduction

The structure of the compression wave generated when a high-speed train enters a tunnel depends critically on tunnel portal geometry. The wave amplitude increases approximately as U^2 for a train travelling at speed U, and the initial thickness of the compression wave front decreases like $1/M$, where $M = U/c_0$ is the train Mach number (c_0 being the mean sound speed in air) [1–4]. Both of these effects tend to exacerbate nonlinear steepening of the wave front in a long tunnel, especially in modern tunnels with concrete slab tracks, which are effectively 'acoustically smooth'

*Corresponding author. Tel.: +1-617-484-0656; fax: +1-617-353-5866.
E-mail address: mshowe@bu.edu (M.S. Howe).

0022-460X/$ - see front matter © 2004 Elsevier Ltd. All rights reserved.
doi:10.1016/j.jsv.2004.01.039

and offer negligible attenuation of the advancing wave front relative to that produced by conventional ballasted track. For long tunnels and train speeds U exceeding about 200 kph, a loud and startling acoustic 'bang' (the 'micro-pressure wave') is frequently radiated out of the distant tunnel exit when the compression wave arrives [1,3,5–7]; the amplitude of this bang is proportional to the wave front steepness of the arriving compression wave.

Nonlinear steepening in a long tunnel is inhibited by diffusive wave thickening produced by dissipation, provided the initial thickness of the compression wave is sufficiently large [1]. The dissipation is small in tunnels with concrete slab-track, and it is then usual to suppress nonlinear steepening by attempting to greatly increase the *initial* 'rise time' of the compression wave. This is done by modifying the tunnel portal where the train enters. The least costly portal modification consists of the tunnel entrance 'hood', which is a thin-walled, cylindrical extension of the tunnel, usually provided with a sequence of open 'windows' that permit the release of high-pressure air produced by an entering train. An alternative modification is the *flared* portal, which has been examined theoretically by Howe [8] and experimentally by Howe et al. [9]. Fig. 1(a) illustrates schematically a uniform tunnel with an integrated flared opening section of length ℓ. Such a portal behaves optimally when the profile of the compression wave produced by an entering train increases *linearly* with time; for a hood of length ℓ this linearly increasing wave front would have thickness $\sim \ell/M$, which is several times the hood length ℓ, because typically $M \sim 0.25$ for high-speed operations.

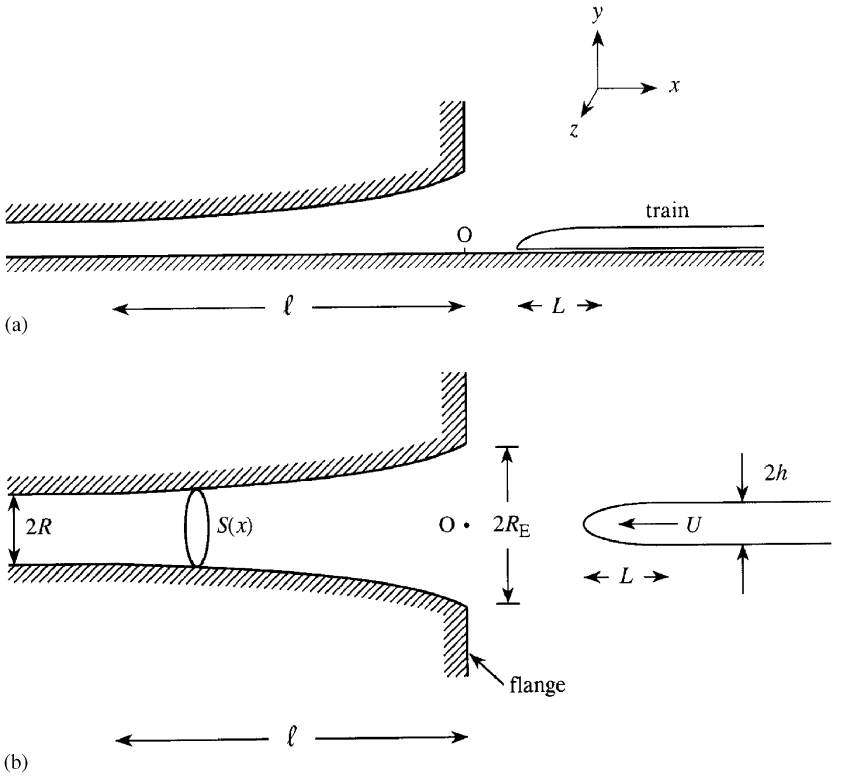

Fig. 1. (a) Train entering a tunnel with a flared portal of length ℓ; (b) axisymmetric flared portal with infinite flange.

Experimental studies of hood design are frequently performed at model scale using axisymmetric tunnel models. The experiments described in Ref. [9] involved an axisymmetric flared tunnel portal of the type illustrated in Fig. 1(b). The model train was also axisymmetric and was projected at high speed into the tunnel along a guide wire stretched along the tunnel axis and passing through a cylindrical axisymmetric bore hole drilled in the model train (see Ref. [9] for a detailed description of the experiment and experimental procedure). The present discussion will be framed in terms of this model configuration, but the results should be applicable also for more general tunnel and portal cross-sections.

It was shown in Ref. [8] that a flared portal of length ℓ behaves optimally (produces a linearly increasing pressure across the compression wave front) provided its cross-sectional area $S(x)$ varies with distance x along its axis according to

$$\frac{S(x)}{\mathscr{A}} = 1 \Big/ \left[\frac{\mathscr{A}}{\mathscr{A}_E} - \frac{x}{\ell}\left(1 - \frac{\mathscr{A}}{\mathscr{A}_E}\right)\right], \quad -\ell < x < 0. \tag{1}$$

In this formula the coordinate origin is at O in the entrance plane of the flared portal (see Fig. 1(b)), with the negative x-axis coinciding with the tunnel axis; the tunnel is uniform for $x < -\ell$ with radius R and cross-section $\mathscr{A} = \pi R^2$. $\mathscr{A}_E$ is the cross-sectional area in the entrance plane $x = 0$, and is given in terms of ℓ, R and $\mathscr{A}$ by

$$\frac{\mathscr{A}_E}{\mathscr{A}} = \left(\frac{\ell}{2R}\right)^{2/3}\left[\left(1 + \sqrt{1 - \left(\frac{2R}{3\sqrt{3}\ell}\right)^2}\right)^{1/3} + \left(1 - \sqrt{1 - \left(\frac{2R}{3\sqrt{3}\ell}\right)^2}\right)^{1/3}\right]^2, \tag{2}$$

provided that $\ell > 2R/3\sqrt{3} \approx 0.385R$.

In the model scale tests described in Ref. [9] the tunnel and portal dimensions were

$$R = 5\,\text{cm}, \quad \ell = 50\,\text{cm}, \quad \mathscr{A}_E/\mathscr{A} = 5.35, \quad R_E/R = 2.31, \tag{3}$$

where R_E is the entrance-plane radius (so that $\mathscr{A}_E = \pi R_E^2$). The axisymmetric model train used in the experiments had an ellipsoidal nose profile obtained by rotating the curve $y = h\sqrt{(x/L)(2 - x/L)}$, $0 < x < L$ about the x-axis. The cross-sectional area of the train $\mathscr{A}_T(x)$ at distance x from the nose tip is therefore given by

$$\frac{\mathscr{A}_T(x)}{\mathscr{A}_0} = \begin{cases} \frac{x}{L}\left(2 - \frac{x}{L}\right), & 0 < x < L, \\ 1, & x > L, \end{cases} \tag{4}$$

where $\mathscr{A}_0 = \pi h^2$, and

$$h = 2.235\,\text{cm}, \quad L = 11.18\,\text{cm}. \tag{5}$$

The tail of the model train has an identical ellipsoidal shape, and the overall length of the train was 91.5 cm.

The pressure rise across the wave front is given approximately by [8,9]

$$\Delta p = \frac{\rho_0 U^2}{(1 - M^2)}\frac{\mathscr{A}_0}{\mathscr{A}}\left(1 + \frac{\mathscr{A}_0}{\mathscr{A}}\right). \tag{6}$$

Typical measured values (from Ref. [9]) of the nondimensional pressure $p/\Delta p$ (open triangles, $\triangle$) and 'pressure gradient' $R(\partial p/\partial t)/U\Delta p$ (solid circles, $\bullet$) are plotted in Fig. 2 against the nondimensional retarded time $U[t]/R \approx U(t + x/c_0)/R$ (see Section 2) for the optimized model scale portal and tunnel with dimensions (3), when the train with nose profile defined by Eqs. (4) and (5) is projected into the tunnel along the axis at $U = 294$ kph ($M = 0.24$) and the nose crosses the entrance plane $x = 0$ at $t = 0$. The measurements were made in the tunnel at a distance of 1.5 m from the portal entrance plane; the pressure rises linearly across the wave front over $0 < U[t]/R < 10 \equiv \ell/R$, during the retarded time in which the train nose traverses the length of the flared portal.

In this paper we examine theoretically how this optimal behaviour of the flared portal is modified when the smoothly profiled entrance is replaced by a step-wise series of coaxial cylindrical sections, as indicated schematically in Fig. 3, which illustrates the case where the flared profile (broken line curves) is replaced by three cylindrical sections of equal axial length. This type of configuration would arise at full scale when, for reasons of economy, the tunnel portal is constructed from sectionally cylindrical components. We shall examine the properties of the compression wave profile generated when the train enters a flared portal constructed in this step-wise fashion, and in particular determine the minimum number of steps that will supply an acceptable approximation to the ideal linear pressure rise across the compression wave front.

The relevant formulae from the theory of compression wave formation are recalled in Section 2. In Section 3 the numerical procedure for analysing the sectionally cylindrical portal is discussed. Numerical results are presented in Section 4. These suggest that a hood with four or more steps of equal length can be expected to provide smooth and environmentally acceptable compression wave profiles, and that it is now appropriate to confirm this conclusion by experiment.

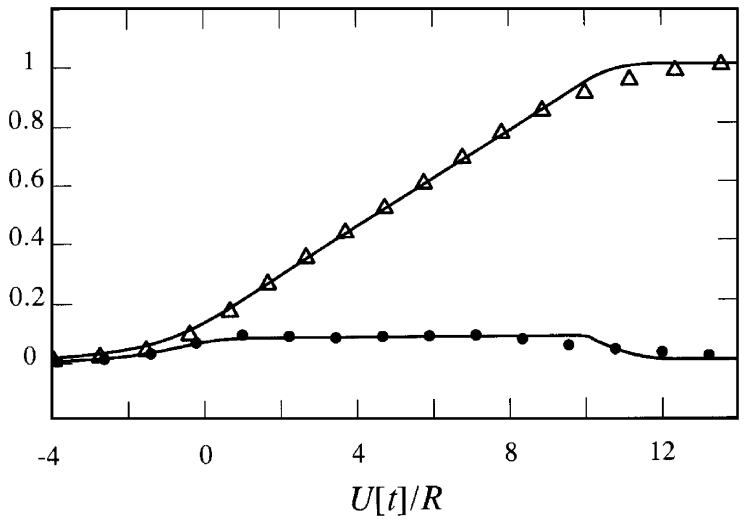

Fig. 2. Calculated (——) and measured values of the nondimensional compression wave pressure ($\triangle\ \triangle\ \triangle$) and pressure gradient ($\bullet\ \bullet\ \bullet$), $p\Big/\frac{\rho_0 U^2}{(1-M^2)}\frac{\mathscr{A}_0}{\mathscr{A}}\left(1+\frac{\mathscr{A}_0}{\mathscr{A}}\right)$, $\frac{\partial p}{\partial t}\Big/\frac{\rho_0 U^3}{R(1-M^2)}\frac{\mathscr{A}_0}{\mathscr{A}}\left(1+\frac{\mathscr{A}_0}{\mathscr{A}}\right)$ produced when the model scale train with the ellipsoidal nosed defined by Eqs. (4) and (5) enters the flared portal and tunnel with dimensions (3) at $U = 294$ kph.

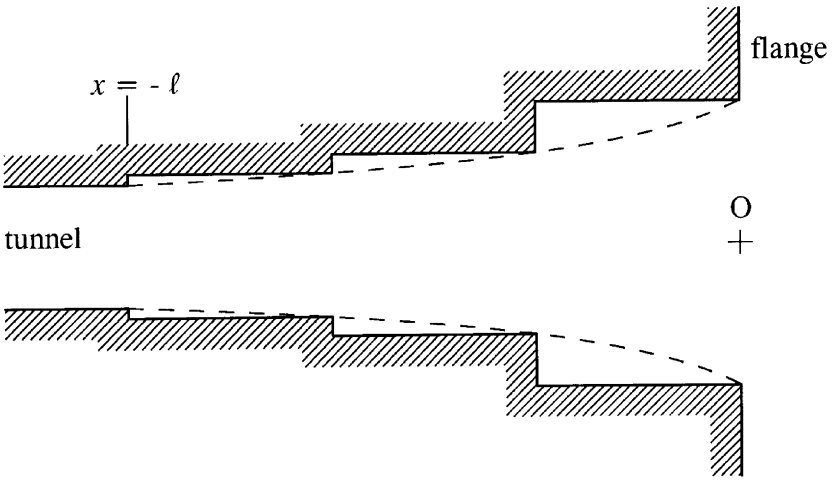

Fig. 3. Approximation to an optimally flared entrance portal by three cylindrical sections of equal axial extent.

2. Analytical representation of the compression wave

The compression wave radiated ahead of the train as it enters the portal and tunnel can be attributed to two principal sources: (i) the piston effect of the 'monopole' displacement of air by the train plus the 'dipole' contribution caused by the pressure rise over the train nose, and (ii) the aerodynamic sound produced by separated flow to the rear of the train nose [10]. For the flared portal the experiments in Ref. [9] confirmed that the contribution from separation becomes important only after the train nose has passed through the portal and into the uniform section of the tunnel, and it therefore influences only the 'late time' behaviour of the wave, to the rear of the wave front.

The detailed characteristics of the wave front are controlled by the 'piston' source (1). In the tunnel region just ahead of the train, *before* the onset of nonlinear steepening, this contribution to the compression wave pressure $p(x,t)$ can be expressed in the form [4,9]

$$p(x,t) \approx \frac{\rho_0 U^2}{\mathscr{A}(1-M^2)}\left(1+\frac{\mathscr{A}_0}{\mathscr{A}}\right)\int_{-\infty}^{\infty}\frac{\partial \mathscr{A}_T}{\partial x'}\,(x'+U[t])\,\frac{\partial \varphi^*}{\partial x'}(x',0,0)\,\mathrm{d}x', \tag{7}$$

where $[t]=t+(x-\ell')/c_0$ is the effective retarded time, and the front of the train is assumed to pierce the entrance plane of the portal at time $t=0$. The length ℓ' is the 'end correction' of the tunnel portal [11,12], and $\varphi^*(\mathbf{x})$ is an auxiliary, harmonic function that depends on the shape of the portal, and has the simple physical interpretation as the velocity potential of ideal, incompressible flow out of the tunnel portal normalized such that (when the 'flange' in Figs. 1 and 3 is large)

$$\varphi^*(\mathbf{x}) \approx \begin{cases} x-\ell' & \text{as } x\to-\infty \text{ inside the tunnel,} \\ -\mathscr{A}/2\pi|\mathbf{x}| & \text{as } |\mathbf{x}|\to\infty \text{ outside the tunnel.} \end{cases} \tag{8}$$

Approximation (7) for the compression wave is applicable when the train 'blockage' $\mathscr{A}_0/\mathscr{A}<0.22$ [9] and provided the portal of length ℓ can be regarded as acoustically compact, i.e. when ℓ is small compared to the thickness of the compression wave front. For a portal optimized in accordance with Eqs. (1) and (2), the wave front thickness $\sim \ell/M$, so that the portal may be regarded as compact provided the train Mach number is small enough. The experiments reported in Ref. [9] confirmed the validity of this conclusion for M as large as 0.25 ($U \sim 300$ kph); in this paper we shall continue to assume that the portal length ℓ is compact.

For the optimally flared portal (with a 'large' flange, as in Fig. 1) the cross-sectional area $S(x)$ varies 'slowly' and in the neighbourhood of the tunnel axis $\varphi^*(\mathbf{x})$ is well approximated by [8,9]

$$\varphi^*(\mathbf{x}) = \begin{cases} -R\sqrt{\frac{\mathscr{A}}{\mathscr{A}_E}} + \mathscr{A}\int_0^x \frac{\mathrm{d}\xi}{S(\xi)}, & x<0, \\ -\frac{R\mathscr{A}}{\mathscr{A}_E}\left[\left(\frac{\mathscr{A}_E}{\mathscr{A}}+\frac{x^2}{R^2}\right)^{1/2} - \frac{x}{R}\right], & x>0. \end{cases} \tag{9}$$

The formula for $x>0$ coincides with the potential produced by a 'baffled' piston of radius R_E and normal velocity $\mathscr{A}/\mathscr{A}_E$ in the exit plane $x=0$. For optimal and nonoptimal portals the end correction ℓ' is given by

$$\ell' = R\sqrt{\frac{\mathscr{A}}{\mathscr{A}_E}} + \int_{-\infty}^{0}\left(\frac{\partial\varphi^*}{\partial x}(x,0,0)-1\right)\mathrm{d}x. \tag{10}$$

The integrand in representation (7) of the compression wave vanishes except in the vicinities of the nose and tail of the train, where $\partial\mathscr{A}_T/\partial x' \neq 0$. The compression wave is generated when the train nose enters the tunnel, and for the purpose of its calculation we may ignore the contribution from the tail, and formally assume the train to be infinitely long, so that the integrand in Eq. (7) is only nonzero in the neighbourhood of the nose. When the nose is fully within the tunnel, we can set $\partial\varphi^*/\partial x' = 1$ in the integral; Eq. (7) then yields the overall pressure rise across the wave front given above in Eq. (6).

The solid curves in Fig. 2 represent predictions of p and $\partial p/\partial t$ from Eq. (7) compared with the experiment of Ref. [9] discussed in Section 1. Theory and experiment are evidently in excellent accord.

3. Numerical evaluation of $\varphi^*(\mathbf{x})$

Representation (7) of the compression wave pressure is also applicable to the step-profiled tunnel portal, and the harmonic function $\varphi^*(\mathbf{x})$ continues to satisfy conditions (8), although in general the value of the end correction ℓ' will vary with the number of steps. The function $\varphi^*(\mathbf{x})$ is the *axisymmetric* solution of Laplace's equation satisfying the asymptotic relations (8) (describing steady, irrotational flow from the portal) and must be determined numerically. It is convenient to do this by first computing the corresponding Stokes stream function $\psi^* \equiv \psi^*(x,r)$, $r=(y^2+z^2)^{1/2}$ [13,14], in terms of which

$$\frac{\partial\varphi^*}{\partial x} = \frac{1}{r}\frac{\partial\psi^*}{\partial r}, \quad \frac{\partial\varphi^*}{\partial r} = -\frac{1}{r}\frac{\partial\psi^*}{\partial x}. \tag{11}$$

For irrotational flow ψ^* satisfies

$$\frac{\partial^2\psi^*}{\partial x^2}+\frac{\partial^2\psi^*}{\partial r^2}-\frac{1}{r}\frac{\partial\psi^*}{\partial r}=0. \tag{12}$$

The stream function assumes constant values on the axisymmetric 'stream surfaces' of the hypothetical flow from the portal. The first condition (of uniform mean flow) in Eq. (8) implies that

$$\psi^*\to\frac{r^2}{2},\quad 0<r<R\quad\text{as } x\to-\infty \text{ in the tunnel.} \tag{13}$$

Thus, $\psi^*=0$ on the axis $r=0$ of the tunnel, and assumes the constant value $\psi^*=R^2/2$ on the tunnel and portal wall. To a good approximation the flow from the portal entrance plane ($x=0$) described by φ^* may also be assumed to be uniform, in which case continuity implies that

$$\psi^*=\frac{\mathscr{A}}{\mathscr{A}_E}\frac{r^2}{2},\quad 0<r<R_E\quad\text{at } x=0. \tag{14}$$

To obtain a numerical solution of Eq. (12) the asymptotic condition (13) (which is actually attained exponentially fast with distance into the tunnel) will be applied at one tunnel diameter from the inner end of the portal (i.e. at $x=-\ell-2R$). Then, Eq. (12) is to be solved within the domain of the (x,r)-plane illustrated in Fig. 4(a) for the case of two cylindrical sections; the figure shows the prescribed values of ψ^* at all points of the domain boundary. The solution can be found using a conventional finite difference approximation, by covering the integration region with a

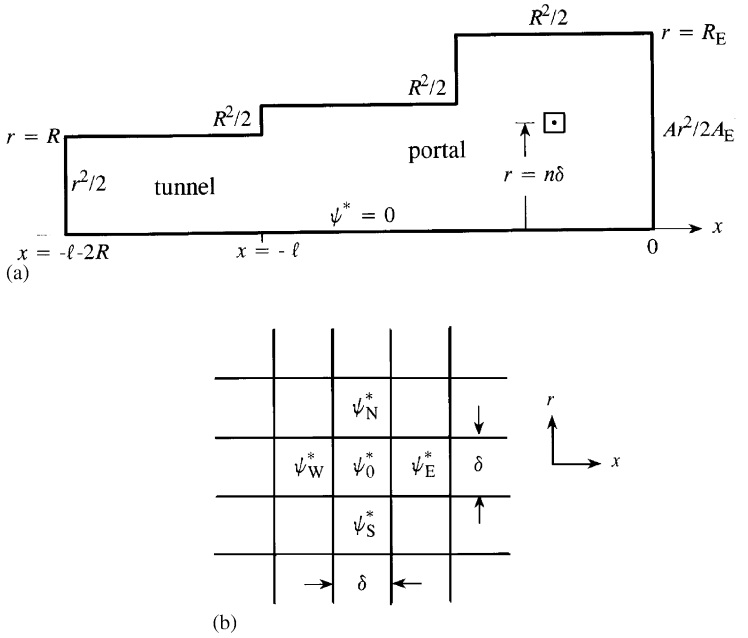

Fig. 4. (a) The boundary values and numerical integration domain for Eq. (12) satisfied by the Stokes stream function $\psi^*(x,r)$ when the flared portal is approximated by two steps. (b) Illustrating the definitions of ψ^*_N, ψ^*_S, ψ^*_E, ψ^*_W in neighbouring spreadsheet cells of side δ that determine the value of ψ^*_0.

grid of squares of side $\delta \ll R$. Following Morishita [15] the calculations can be conveniently and quickly performed using an Excel spreadsheet, in which each spreadsheet cell is identified with a square of the grid. Those cells lying on the boundary of the integration region are filled with the prescribed boundary values of ψ^*. The value $\psi^* = \psi_0^*$ at an interior cell '0', say (see Fig. 4(b)), is related to values in neighbouring cells by the finite difference scheme. In the simplest case Eq. (12) evaluated at the centre of cell 0 becomes

$$\frac{\psi_E^* - 2\psi_0^* + \psi_W^*}{\delta^2} + \frac{\psi_N^* - 2\psi_0^* + \psi_S^*}{\delta^2} - \frac{1}{n\delta}\frac{(\psi_N^* - \psi_S^*)}{2\delta} = 0, \tag{15}$$

where ψ_N^*, ψ_S^*, ψ_E^*, ψ_W^* are the values of ψ^* in the neighbouring cells shown in Fig. 4(b), and $r = n\delta$, $n = 1, 2, 3, \ldots$ is the radial distance of the centre of cell 0 from the axis of symmetry. Hence,

$$\psi_0^* = \frac{1}{4}\left\{\left(1 - \frac{1}{2n}\right)\psi_N^* + \psi_E^* + \psi_W^* + \left(1 + \frac{1}{2n}\right)\psi_S^*\right\}. \tag{16}$$

This formula is inserted into each interior cell of the spreadsheet and the Excel program is then run in 'iterative mode' until calculated cell values cease to change relative to a predefined level of accuracy. The number of iterations depends on the ratio δ/R and on the level of accuracy prescribed for the spreadsheet calculations. In the results presented below we have taken $\delta/R = 0.01$. Further details of the procedure are discussed in Ref. [16].

4. Numerical results

To evaluate the compression wave pressure from the integral in Eq. (7) the variation of $\partial\varphi^*/\partial x$ is required on the tunnel axis (the x-axis). Typical calculated values of $\partial\varphi^*(x,0,0)/\partial x$ and $\partial^2\varphi^*(x,0,0)/\partial x^2$ are displayed in Fig. 5 for portal configurations involving 2, 3, and 5 step changes in diameter (the values of these functions outside the tunnel, in $x>0$, are defined by the piston approximation of Eq. (9)). Also shown are the corresponding values of these derivatives for the optimally flared portal of Fig. 1(b), calculated from Eq. (9). It is evident that the predictions for the stepped configurations approach the optimal variations as the number of steps increases.

Sample predictions of Eq. (7) of the compression wave pressure p and the pressure gradient $\partial p/\partial t$ are presented in Figs. 6 and 7 for two different model trains with ellipsoidal nose shapes, and for tunnel and portal dimensions given in Eq. (3). In both cases the train enters the tunnel at $U = 294\,\text{kph}$ ($M = 0.24$) at the nondimensional retarded time $U[t]/R \sim 0$ (not exactly 0 because $[t] = t + (x - \ell')/c_0$, where according to Eq. (10) the end correction ℓ' is *negative* and is of order R in absolute value). For the cases illustrated in Fig. 6 the train nose aspect ratio $L/h = 3$, where $h = 2.235\,\text{cm}$, as in Eq. (5), and the train blockage $\mathscr{A}_0/\mathscr{A} = 0.2$. The solid curves show the predicted variations of p and $\partial p/\partial t$ for portals with 3, 5 and 7 steps. The main pressure rise across the wave front is essentially linear with superposed ripples; the amplitude of the ripples decreases as the number of steps increases. In all cases the main pressure rise occurs over a nondimensional time interval $Ut/R \sim 10$ during which the train nose traverses the flared section, so that the thickness of the compression wave front $\sim 10R/M = \ell/M$, which is about four times the length of the portal. For the optimally flared, smooth-walled portal defined by Eqs. (1) and (2), the

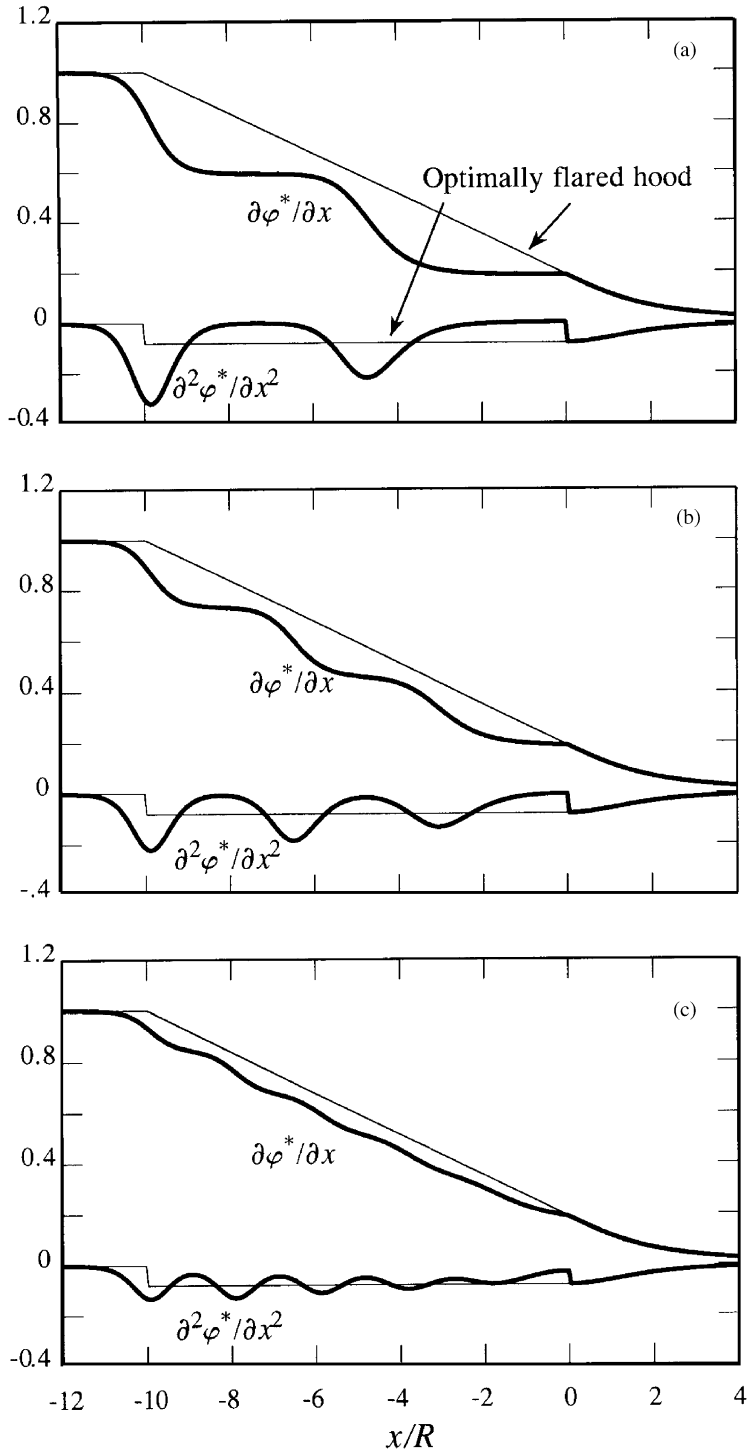

Fig. 5. Calculated values of $\partial\varphi^*/\partial x$ and $\partial^2\varphi^*/\partial x^2$ on the axis of the tunnel and portal for (a) 2, (b) 3 and (c) 5 step configurations.

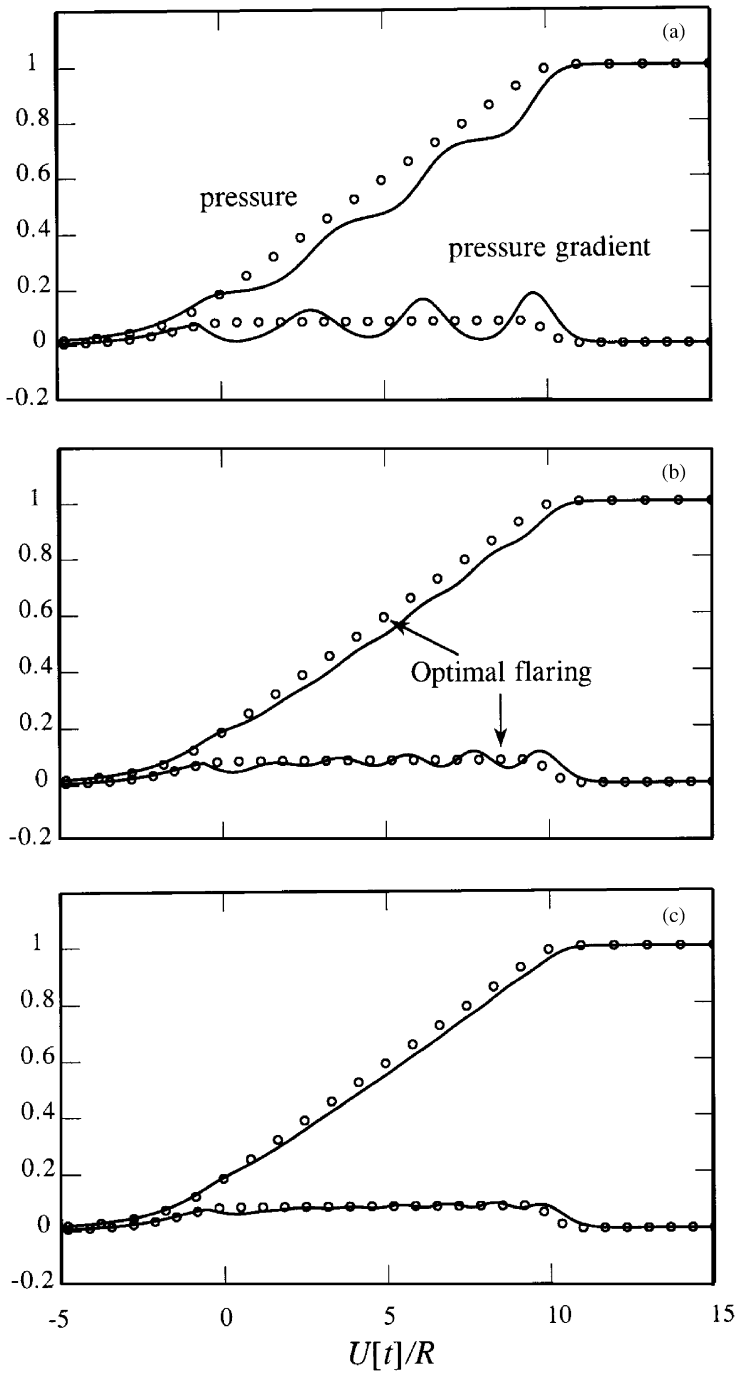

Fig. 6. Calculated nondimensional pressure and pressure gradient (——), $p\Big/\frac{\rho_0 U^2}{(1-M^2)}\frac{\mathscr{A}_0}{\mathscr{A}}\left(1+\frac{\mathscr{A}_0}{\mathscr{A}}\right)$, $\frac{\partial p}{\partial t}\Big/\frac{\rho_0 U^3}{R(1-M^2)}\frac{\mathscr{A}_0}{\mathscr{A}}\left(1+\frac{\mathscr{A}_0}{\mathscr{A}}\right)$, for a portal with (a) 3, (b) 5 and (c) 7 steps and overall dimensions (3), compared with predictions (○ ○ ○) for an optimally flared portal for an ellipsoidal train nose (4) with $h = 2.235\,\text{cm}$, $L/h = 3$ and $U = 294\,\text{kph}$.

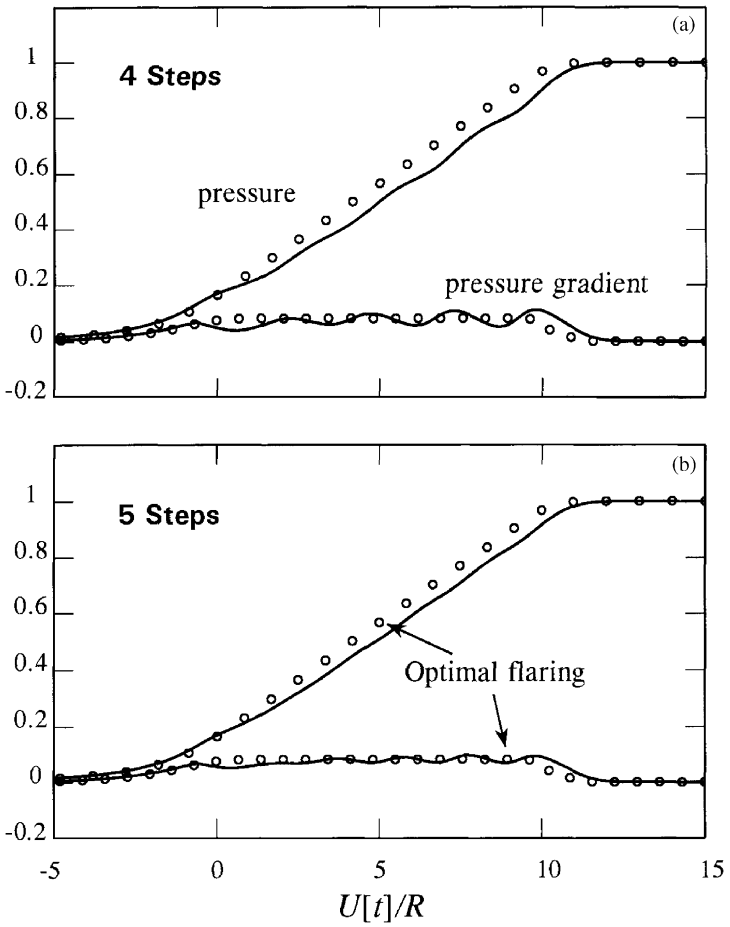

Fig. 7. Calculated nondimensional pressure and pressure gradient (——), $p\Big/\frac{\rho_0 U^2}{(1-M^2)}\frac{\mathscr{A}_0}{\mathscr{A}}\left(1+\frac{\mathscr{A}_0}{\mathscr{A}}\right)$, $\frac{\partial p}{\partial t}\Big/\frac{\rho_0 U^3}{R(1-M^2)}\frac{\mathscr{A}_0}{\mathscr{A}}\left(1+\frac{\mathscr{A}_0}{\mathscr{A}}\right)$, for a portal with (a) 4 and (b) 5 steps and overall dimensions (3), compared with predictions (○ ○ ○) for an optimally flared portal for an ellipsoidal train nose (4) with $h = 2.235\,\text{cm}$, $L/h = 5$ and $U = 294\,\text{kph}$.

pressure rise is almost exactly linear over the interval $0 < U[t]/R < 10$; as shown by the open-circle curves in the figures. At seven steps there is very little practical difference between the smooth and stepped portal predictions.

The train nose is acoustically equivalent to a distribution of monopole and dipole sources extending over the nose region, where the train cross-sectional area $\mathscr{A}_T$ is varying. Thus, increasing the aspect ratio L/h for a fixed value of the train radius h reduces the strength of these sources per unit length of nose, and this would be expected to reduce the amplitude of the pressure fluctuations in the main pressure rise across the wave front. This is clear from an inspection of Fig. 7, where results are shown for 4 and 5 step approximations for the same train, tunnel and Mach number, but with the aspect ratio increased to $L/h = 5$ (corresponding to the experimental data in Fig. 2 for the smooth-walled portal). It is clear that the five-step approximation now furnishes essentially the same linear pressure rise as the optimally flared portal.

5. Conclusion

Optimal flaring of a tunnel portal produces a linear rise in pressure over the front of the compression wave generated by a high-speed train, with a total wave front thickness approximately equal to ℓ/M. The calculations presented in this paper indicate that the pressure rise remains essentially linear with superposed fluctuations when the flared portal is fabricated using discrete, coaxial cylindrical sections to approximate the ideally flared geometry. These fluctuations may be attributed to the interaction of the train nose 'sources' with successive changes in portal geometry where the tunnel diameter changes between adjacent sections of the portal. The amplitude of these fluctuations is reduced when the length of the train nose L is increased, so that for a given train speed, successive interactions take place over a longer interval of time. Our numerical results indicate that a flared portal is likely to be well approximated by a stepped portal of three or four cylindrical sections for train Mach numbers up to about 0.25 ($U \sim 300$ kph). This conclusion should now be confirmed by experiment. At higher train Mach numbers the influence of air compressibility in the portal (neglected in the present analysis) will become important, and must be expected to modify the predictions of this paper.

Acknowledgements

The work reported in this paper is sponsored by the Railway Technical Research Institute, Tokyo, Japan.

References

[1] S. Ozawa, T. Maeda, T. Matsumura, K. Uchida, H. Kajiyama, K. Tanemoto, Countermeasures to reduce micro-pressure waves radiating from exits of Shinkansen tunnels, in: A. Haerter (Ed.), *Aerodynamics and Ventilation of Vehicle Tunnels*, Elsevier, Amsterdam, 1991, pp. 253–266.

[2] S. Ozawa, T. Maeda, T. Matsumura, K. Nakatani, K Uchida, Distortion of compression wave during propagation along Shinkansen tunnel, *Proceedings of the Eighth International Conference on Aerodynamics and Ventilation of Vehicle Tunnels*, Liverpool, UK, 6–8 July 1994, ME Publications, London, 1994, pp. 211–226.

[3] T. Maeda, Micropressure waves radiating from a Shinkansen tunnel portal, in: V.V. Krylov (Ed.), *Noise and Vibration from High Speed Trains*, Thomas Telford, London, 2002 (Chapter 7).

[4] M.S. Howe, The compression wave produced by a high-speed train entering a tunnel, *Proceedings of the Royal Society A* 454 (1998) 1523–1534.

[5] S. Ozawa, T. Maeda, Model experiment on reduction of micro-pressure wave radiated from tunnel exit, *Proceedings of the International Symposium on Scale Modeling*, Japan Society of Mechanical Engineers, Tokyo, 18–22 July, 1988.

[6] S. Ozawa, T. Maeda, Tunnel entrance hoods for reduction of micro-pressure wave, *Quarterly Report of the Railway Technical Research Institute* 29 (3) (1988) 134–139.

[7] R. Gregoire, J.M. Rety, V. Moriniere, M. Bellenoue, T. Kageyama, Experimental study (scale 1/70th) and numerical simulations of the generation of pressure waves and micro-pressure waves due to high-speed train-tunnel entry, *Proceedings of the Ninth International Conference on Aerodynamics and Ventilation of Vehicle Tunnels*, Aosta Valley, Italy, 6–8 October 1997, ME Publications, London, 1997, pp. 877–902.

[8] M.S. Howe, On the compression wave generated when a high-speed train enters a tunnel with a flared portal, *Journal of Fluids and Structures* 13 (1999) 481–498.

[9] M.S. Howe, M. Iida, T. Fukuda, T. Maeda, Theoretical and experimental investigation of the compression wave generated by a train entering a tunnel with a flared portal, *Journal of Fluid Mechanics* 425 (2000) 111–132.
[10] M.S. Howe, M. Iida, Influence of separation on the compression wave generated by a train entering a tunnel, *International Journal of Aeroacoustics* 2 (2003) 13–33.
[11] Lord Rayleigh, *The Theory of Sound*, Vol. 2, Macmillan, London, 1926.
[12] M.S. Howe, *Acoustics of Fluid–Structure Interactions*, Cambridge University Press, Cambridge, 1998.
[13] H. Lamb, *Hydrodynamics*, 6th ed., Cambridge University Press, Cambridge, 1932 (reprinted 1993).
[14] G.K. Batchelor, *An Introduction to Fluid Dynamics*, Cambridge University Press, Cambridge, 1967.
[15] E. Morishita, Spreadsheet fluid dynamics, *Journal of Aircraft* 36 (1999) 720–723.
[16] A. Winslow, Concentric step configurations approximating the ideal profile of a flared portal of a high-speed train tunnel, Department of Aerospace and Mechanical Engineering, Boston University, Summer Project Report, 2003.